Finite-size effects in thin Ag-Mn spin-glass layers

R. Stubi,* J. A. Cowen, L. Hoines, M. L. Wilson, W. A. Fowler, and J. Bass
Department of Physics and Astronomy and Center for Fundamental Materials Research, Michigan State University, East Lansing, Michigan 48824-1116
(Received 18 March 1991; Revised Manuscript received 29 July 1991)

Measurements of the quasistatic spin-freezing temperature T_f, as a function of spin-glass layer thickness, $W_{\text{Ag-Mn}}$, are presented for multilayer samples of the spin-glass $Ag_{1-x}Mn_x$ ($x=0.04$ and 0.09) alternated with interlayers of Ag or Cu having thickness $W_{\text{il}}=30$ nm, a value large enough to magnetically decouple the spin-glass layers. The values of T_f are independent of whether the interlayer metal is Ag or Cu, and thus insensitive to grain sizes and structural details of spin-glass–interlayer interfaces. To within experimental uncertainty, for a given value of W_{SG}, the ratio T_f/T_f^b (T_f^b is the bulk transition temperature for a given x) for $Ag_{1-x}Mn_x$ is independent of x and the same as was previously found for Cu-Mn. The data for thin ($W_{\text{SG}} \leq 10$ nm) spin-glass layers are compatible with the predictions of the Fisher-Huse droplet-excitation model. Under some circumstances, large-angle x-ray scattering is shown to directly measure the layer thickness of the thinner of the two constituents of a multilayer sample.

I. INTRODUCTION

Modern techniques for fabricating monatomic layers and multilayer systems make it possible to study finite-size effects and three-dimensional (3D) to 2D crossover behavior in magnetic systems. A fair amount is known about finite-size effects in systems with long-range order such as ferromagnets;[1] rather less is known about disordered systems such as spin glasses (SG's). We and others recently showed[2–5] that as the thickness W_{SG} of layers of the SG $Cu_{1-x}Mn_x$ ($0.04 \leq x \leq 0.14$) is reduced, the quasistatic spin-freezing temperature T_f [defined as the location of the peak in the zero-field-cooled (ZFC) linear magnetic susceptibility for a measuring time per data point of several minutes] decreases systematically, approaching 0 K as W_{SG} approaches 0 nm. In the present paper we show that a second spin glass, Ag-Mn, displays qualitatively and quantitatively similar behavior to Cu-Mn.

In this section, we limit ourselves to reviewing previous finite-size-effect studies of metallic SG's and the models with which we will compare our data. The reader interested in a more complete background and discussion of related issues, as well as a justification for finite-size studies of T_f in metallic and nonmetallic SG's, is referred to Ref. 4. Aside from a brief mention below of the nonlinear susceptibility, and of how the dependence of T_f on measuring time and the aging behavior in $Cu_{1-x}Mn_x$ vary with W_{SG}, we focus upon changes in T_f with decreasing W_{SG}. It is important to emphasize that T_f measures only a dynamic property of the SG and that, to the extent that a SG can be said to undergo a true phase transition, it does so only in the limit $\tau \rightarrow \infty$. In Sec. II, we describe sample preparation and characterization. In Sec. III we present and analyze our Ag-Mn data and compare them with previous results for Cu-Mn. Section IV contains a summary and conclusions.

In the first published attempt to observe finite-size effects in metallic SG's, Cowen, Kenning, and Slaughter[6] studied T_f as a function of $W_{\text{Cu-Mn}}$ in sputtered multilayer samples (MS's) with $W_{\text{SG}}=1.5$ nm of $Cu_{0.93}Mn_{0.07}$ alternated with interlayer thicknesses of $W_{\text{il}}=1.5$ to 9 nm of Cu or with $W_{\text{SG}}=10$ to 0.5 nm of Cu-Mn alternated with $W_{\text{il}}=1.2$ nm of Si. They did not find any clear evidence of finite-size effects, and we now know that their values of W_{il} were too small to magnetically decouple the SG layers.

The first definitive demonstration that T_f decreases systematically with decreasing $W_{\text{Cu-Mn}}$ for magnetically decoupled SG layers was made by Kenning, Slaughter and Cowen[2] on sputtered MS's with $W_{\text{Cu-Mn}}=2$ to 1000 nm alternated with 7 nm of Si. They reported that all of their data could be fit with the finite-size scaling equation[7]

$$(T_f^b - T_f)/T_f^b = (W_{\text{SG}}/W_c)^{-1/\nu}, \quad (1)$$

where T_f^b is the bulk transition temperature for a given x, W_c is the SG width at which $T_f=0$ K, and ν is a constant. For $Cu_{1-x}Mn_x$/Si MS's with $0.04 \leq x \leq 0.14$, Kenning and co-workers found[2,4] that $W_c \approx 3.5$ nm and $\nu \approx 1.6 \pm 0.3$; this latter value is slightly larger than the value of $\nu=1.3\pm0.2$ found from nonlinear susceptibility measurements.[8] The ability of Eq. (1) to fit data over very wide ranges of W_{SG} is surprising, since Eq. (1) is expected to be valid only near T_f^b.[7]

Cowen, Kenning, and Bass[3] and Kenning *et al.*[4] subsequently found that the values of T_f for Cu-Mn/Cu MS's decreased somewhat less rapidly with decreasing W_{SG} than those for Cu-Mn/Si MS's. The Cu-Mn/Cu MS data were also compatible with Eq. (1), but with $W_c \approx 1$ nm and $\nu \approx 1.2 \pm 0.3$. Kenning *et al.*[4] provided evidence that the larger value of W_c for Cu-Mn/Si was due, at least in part, to contamination of the Cu-Mn by Si. Stubi *et al.*[9] later showed that cooling the sample substrates to room temperature or below during sputtering reduced the

value of W_c derived for Cu-Mn/Si MS's toward that found for Cu-Mn/Cu MS's.

Recently, Gavrin *et al.*[5] reported that Cu-Mn/Al_2O_3 MS with W_{SG} extending down to 6 nm showed decreases in T_f with decreasing $W_{Cu\text{-}Mn}$ comparable to those found for Cu-Mn/Si, and Vranken and co-workers[10,11] reported similar decreases for Au-Fe single films with W_{SG} down to ≈ 6 nm. Fitting their $Cu_{0.92}Mn_{0.08}/Al_2O_3$ MS data to Eq. (1) for W_{SG} up to 200 nm, Gavrin *et al.* derived a value of $W_c \approx 2$ nm and $\nu = 1.6 \pm 0.2$. Also using Eq. (1), Vranken *et al.* initially reported obtaining $W_c \approx 10$ nm for $Au_{0.99}Fe_{0.01}$,[9] but subsequently found that thin-film data for $Au_{0.95}Fe_{0.05}$ deviated from Eq. (1) for $W_{SG} \leq 10$ nm.[10]

Stimulated by the initial data of Kenning, Slaughter, and Cowen[2] Fisher and Huse[12] examined the 3D to 2D crossover behavior expected in Cu-Mn in terms of a droplet excitation model. For T_f near T_f^b, assuming that the lower critical dimension[7] d_l lies between 3 and 2, they derived an equation similar to Eq. (1), except multiplied by a factor logarithmic in the measuring time τ;

$$\frac{T_f^b - T_f(\tau)}{T_f^b} \propto W_{SG}^{-(1/\nu_3)} \left[\ln \left(\frac{\tau}{W_{SG}^{z_3}} \right) \right]^{[\psi_3 + \nu_2 \psi_2 \theta_3)\nu_3]^{-1}} . \quad (2)$$

Here subscripts denote dimensionality, z is the standard exponent for dynamic critical scaling, ψ and θ are scaling exponents for activation barriers and free energies, respectively, and W_{SG} and τ are measured in terms of a microscopic length and a microscopic time, respectively.[12] Our thick W_{SG} data are not accurate enough to distinguish between Eqs. (1) and (2).

For W_{SG} thin enough and τ long enough so that $T_f/T_f^b \ll 1$ (but with W_{SG} still larger than the average separation between impurities), Fisher and Huse derived the equation

$$T_f(\tau)/T_f^b \propto \left(\frac{W_{SG}^{\psi_3 + \psi_2 \nu_2 \theta_3}}{\ln \tau} \right)^{(1+\nu_2\psi_2)^{-1}} . \quad (3)$$

For fixed τ, Eq. (3) can be simplified to

$$T_f/T_f^b \propto W_{SG}^a , \quad (4)$$

where the condition[12] $d - 1 \geq \psi \geq \theta$ sets an upper bound of a $\leq \psi_3 \leq 2$. The values of the parameters in Eq. (3)—θ_3, $\psi_2\nu_2$, and especially ψ_3—are all highly uncertain. However, from simulations and experimental data,[8,13,14] we can estimate approximate bounds on these values, $0.2 \leq \theta_3 \leq 0.3$, $1 \leq \psi_2\nu_2 \leq 2.2$, and $0.5 \leq \psi_3 \leq 1$, which lead to an estimate of $0.3 \leq a \leq 0.65$. The only previous measurement of a from size effects is that by Kenning *et al.*,[4] who found $a \approx 0.5 \pm 0.1$ for Cu-Mn/Cu MS's with 2 nm $\leq W_{Cu\text{-}Mn} < 20$ nm. As their data extended only to $T_f/T_f^b \approx 0.3$, they did not reach $T_f/T_f^b \ll 1$.

Studies have also recently been made of effects of SG layer thickness on the high-field nonlinear susceptibility,[5] on how T_f varies with measuring time τ,[14] and on how the relaxation rate varies with W_{SG} for both magnetically isolated and partially recoupled SG layers.[15] These studies provide plausible evidence of 3D to 2D crossover behavior, with the second[14] explicitly suggesting that there is a finite value of W_{SG} below which T_f extrapolates to 0 K in the limit $\tau \rightarrow \infty$.

The foci of the present investigation were (a) to determine whether the behavior of T_f seen in Cu-Mn is also seen in another SG, and (b) to test whether this behavior is sensitive to the interlayer metal. Ag-Mn was chosen as the SG with properties closest to those of Cu-Mn.[16,17] Cu and Ag were chosen as alternative interlayers because (a) they are the host metals of Cu-Mn and Ag-Mn, (b) their electronic structures are almost identical, but (c) their lattice parameters differ enough ($\approx 13\%$) to produce significantly different interface structures and grain sizes in Ag-Mn/Ag and Ag-Mn/Cu MS's.

Some data from this work have already been published elsewhere.[9,18] Complementary "recoupling" experiments on the return to 3D from quasi-2D in both Cu-Mn and Ag-Mn—based MS's when W_{SG} is held constant at 4 nm and W_{il} is reduced from 120 to 1 nm are being published separately.[19]

We previously showed for Cu-Mn/Cu MS's (Ref. 4) that we could rule out, as being of only minor importance, the potentially complicating effects of (a) reduction in the number of nearest Mn neighbors at the surfaces of finite-thickness layers, and (b) "spreading" of Mn out of the Cu-Mn layers and into the Cu during sputtering. The arguments given there apply equally well to the current work on Ag-Mn, and we do not consider these phenomena further. We also showed[4] that the finite-correlation-length spin-density-wave picture of Werner and co-workers[20] did not provide additional insight into our Cu-Mn/Cu data, and the same conclusion follows for the current data. Due to experimental uncertainties in the normalizing values of T_f^b for our Ag-Mn–based data, we limit our comparison of thick W_{SG} data with Eq. (1) to showing that the new data cluster around the fit previously obtained for Cu-Mn–based MS's.[4] For thin W_{SG} data, in contrast, we independently fit our new data with Eq. (4).

II. SAMPLE PREPARATION AND CHARACTERIZATION

A. Sample preparation and T_f^b

The MS samples were prepared by dc sputtering onto Si(001) substrates cooled to just below room temperature as described elsewhere.[3,4,21] To test whether the values of T_f are independent of the specific nature of the interlayer metal, both Ag-Mn/Ag and Ag-Mn/Cu MS's were made. Two nominally identical MS's were sputtered simultaneously onto substrates located symmetrically about the axes of the sputtering targets.

For Cu-Mn samples, we have always found the values of T_f measured on sputtered 500–1000-nm films to be essentially the same as those for shavings taken from the sputtering target, indicating that the Mn content of the films is the same as in the target. To ensure consistency, we took the T_f^b for a given Mn concentration to be the value for the shavings.[4]

For Ag-Mn, in contrast, the values of T_f for sputtered

400–1000-nm-thick films were systematically about 40% lower than those for shavings. The Mn content was found to be uniform throughout the Ag-Mn targets, and to be only little changed after substantial sputtering from the target. We thus concluded that the loss of Mn must be occurring during the sputtering process itself. Varying the sputtering rate from 0.6 to 1.8 nm/sec produced no obvious change in Mn content of the sputtered films, provided that the sputtering pressure was maintained constant. However, increasing the sputtering pressure, while holding the other parameters constant, substantially decreased both the sputtering rate and the Mn content, as shown in Fig. 1. The lighter Mn atoms are apparently scattered more strongly by the Ar atoms of the sputtering gas than are the heavy Ag atoms.

In view of this Mn loss during sputtering, we have chosen the values of T_f^b for the Ag-Mn alloys to be averages of those for 400–1000-nm-thick films. Due to a combination of the angular dependence of the amount of Mn arriving at the substrate noted above, with different locations of different substrates relative to the sputtering gun axis during sputtering, we observed variations around these chosen values. These variations lead to an uncertainty in T_f^b of about $\pm 5\%$ for the $Ag_{0.91}Mn_{0.09}$/Cu MS's and slightly more for the $Ag_{0.96}Mn_{0.04}$/Ag and $Ag_{0.96}Mn_{0.04}$/Cu MS's. From the reproducibility and internal consistency of the data for our Ag-Mn MS's (see Table IV below), we are confident that the Mn loss was the same for all of our sputtered samples to within the percentage uncertainties listed for T_f^b. The specified Mn concentrations of 0.04 and 0.09 were estimated from the known curves of T_f^b vs x for Ag-Mn.[16]

B. X rays and film-thickness determination

Ag-Mn and Ag have nearly the same electron density, and the lattice parameter of Ag does not change appreciably as Mn is added.[22] Multilayer satellites in Ag-Mn/Ag MS's are thus too weak to be seen. The widths of x-ray lines can, however, yield useful information about correlation lengths (which we take to be the average grain sizes) normal to the MS layers. We presume that grain sizes within the layers are comparable to those normal to the layers, but we have not measured the former.

For Ag-Mn/Cu MS's, in contrast, x rays permit the determination of both the bilayer thickness d and average grain sizes normal to the layers. We will show that, in some cases, x rays can also directly yield individual layer thicknesses.

1. Average grain sizes normal to the layers

The first two columns of Tables I–III contain the intended values of W_{SG} and d, respectively, for $Ag_{0.96}Mn_{0.04}$/Ag, $Ag_{0.96}Mn_{0.04}$/Cu, and $Ag_{0.91}Mn_{0.09}$/Cu MS's. The last columns contain the average grain sizes ξ for each of the samples, determined from the standard Scherrer formula as described previously.[4]

Since Ag-Mn and Ag have nearly the same lattice parameters,[22] we expect epitaxial growth at the interfaces, and indeed Table I shows that the grain sizes for Ag-Mn/Ag MS's are ≈ 50 nm, larger than the bilayer thicknesses d of all but the samples with the largest d, and nearly independent of W_{SG}. Similar behavior was also previously found in Cu-Mn/Cu MS's.[4]

The lattice parameters of Ag and Cu, in contrast, differ by about 13%.[22] Here, we expect grain sizes to be bounded by the individual layer thicknesses. The last two columns of Tables II and III show that this expectation is generally valid.

2. Superlattice periodicity

For the Ag-Mn/Cu MS's, columns 3, 4, and 5 in Tables II and III contain the values of d determined, respectively, from the total sample thickness (measured

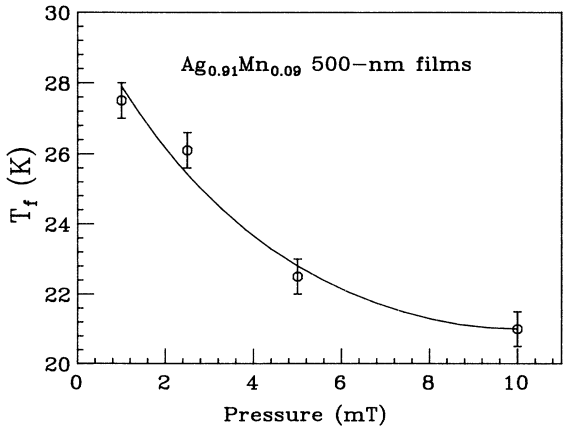

FIG. 1. T_f vs sputtering pressure P_s for 500-nm-thick Ag-Mn films prepared with target voltage and current held fixed. The decrease of T_f with increasing P_s indicates a decreasing fraction of Mn in the sputtered films. The curve is simply a guide to the eye.

TABLE I. Intended SG layer thicknesses W_{SG}; intended bilayer thicknesses d; Dektak-measured bilayer thicknesses d_{Dek}; and x-ray measured crystallite sizes ξ_T, for the $Ag_{0.96}Mn_{0.04}$/Ag MS's. The units are nm and the uncertainties are several percent.

	(Ag–4 at. % Mn)/Ag		
W_{SG}	d	d_{Dek}	ξ_T
100	130	118	50
50	80		48
25	55		48
		56	
12.5	42.5	40	57
		43	
7	37	35	52
5	35	34	64
		37	
3.5	33.5	33	54
2.0	32	31	52
		33.5	

TABLE II. Intended SG layer thicknesses W_{SG}; intended bilayer thicknesses d; Dektak, SAXD, and LAXD measured bilayer thicknesses d_{Dek}, d_{SAXD}, and d_{LAXD} and SG layer thicknesses W_{SG}^{M}; and x-ray measured crystallite sizes $\xi_{Ag\text{-}Mn}$ and ξ_{Cu}, for the separate constituents of the $Ag_{0.96}Mn_{0.04}$/Cu MS's. The units are nm and the uncertainties are several percent.

		$Ag_{0.96}Mn_{0.04}$/Cu					
W_{SG}	d	d_{Dek}	d_{SAXD}	d_{LAXD}	W_{SG}^{M}	$\xi_{Ag\text{-}Mn}$	ξ_{Cu}
100	130					27	24
		142.5					
50	80	77.5					
						31	26
25	55	52					
		54			24.5	18	22
12.5	42.5	40		44.5	10	10	19
				40.5	12	13	31
7	37	37.5					
		38		34.5	6.7	7.7	37
5	35		44	32.5		4.6	19
		36					
3.5	33.5	32.5					
		33		31		2.6	42
2	32	30	38.5	30			32
		31					

with a Dektak IIA profilometer) divided by the number of layers deposited, from small-angle x-ray diffraction (SAXD) and from large-angle x-ray diffraction (LAXD). For the Ag-Mn/Ag MS's, column 3 of Table I contains similar Dektak-determined values. Because of the large value of W_{il} (i.e., 30 nm) needed to magnetically decouple the SG layers, the SAXD satellites occur at rather small angles, and the LAXD satellites appear superimposed upon the diffraction peaks for Ag-Mn and Cu as illustrated in Figs. 2 and 3. Both the small- and large-angle satellites were thus generally few and weak, leading to uncertainties in d_{SAXD} and d_{LAXD} of several percent.

In some circumstances, the satellite structure was dominated not by the oscillations due to the bilayer thickness d, but rather by the "diffraction patterns" from the thinner of the two layers of the MS (in our case, W_{SG}). Figures 4 and 5 illustrate data that directly provide values for W_{SG} (which we designate by W_{SG}^{M}). Although such "diffraction" induced structure has been seen in SAXD data,[5] and is formally contained in the appropriate x-ray equations, the fact that this structure directly yields W_{SG} does not seem to be widely appreciated.

Figure 4 compares data (solid curve) for a $Ag_{0.96}Mn_{0.04}$/Cu (7-nm/30-nm) MS with a calculation (dashed curve) for a single bilayer having a square-wave concentration profile (i.e., N_{SG} layers of the SG with lattice parameter a_{SG}, and N_{IL} layers of the interlayer with lattice parameter a_{IL}). In the solid curve, the bilayer os-

TABLE III. Intended SG layer thicknesses W_{SG}; intended bilayer thicknesses d; Dektak, SAXD, and LAXD measured bilayer thicknesses d_{Dek}, d_{SAXD}, and d_{LAXD} and SG layer thicknesses W_{SG}^{M}; and x-ray measured crystallite sizes $\xi_{Ag\text{-}Mn}$ and ξ_{Cu}, for the separate constituents of the $Ag_{0.91}Mn_{0.09}$/Cu MS's. The units are nm and the uncertainties are several percent.

		$Ag_{0.91}Mn_{0.09}$/Cu					
W_{SG}	d	d_{Dek}	d_{SAXD}	d_{LAXD}	W_{SG}^{M}	$\xi_{Ag\text{-}Mn}$	ξ_{Cu}
500	530	571				49	26
200	230	228				41	11
100	130	134				32	25
50	80	80				30	26
25	55	54.9			26.2	22	27
12.5	42.5	41.3		40.2	11.3	12	23
7	37	34.5		38.7		6.9	25
5	35	36		33.2		5.1	24
4	34	36.2	42.2			4.0	
3.5	33.5	32.9		37.6		3.6	32
2	32	31.8	34.5	30.1			36
1	31	31.4		30.8			20

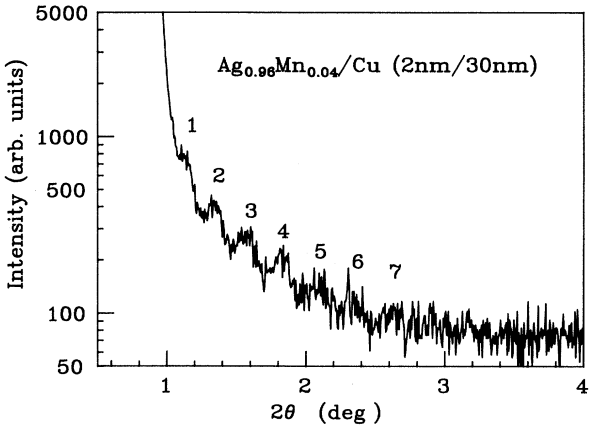

FIG. 2. The SAXD pattern for a $Ag_{0.91}Mn_{0.09}/Cu$ (2-nm/30-nm) MS. The separation between the SAXD satellites determines d.

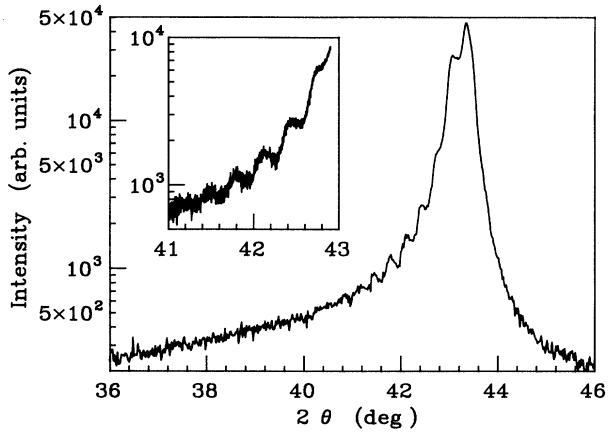

FIG. 3. The LAXD pattern for a $Ag_{0.91}Mn_{0.09}/Cu$ (1-nm/30-nm) MS. The separation between the LAXD satellites determines d. The inset is an expanded view of the region from 41°–43° using the same units as the main figure.

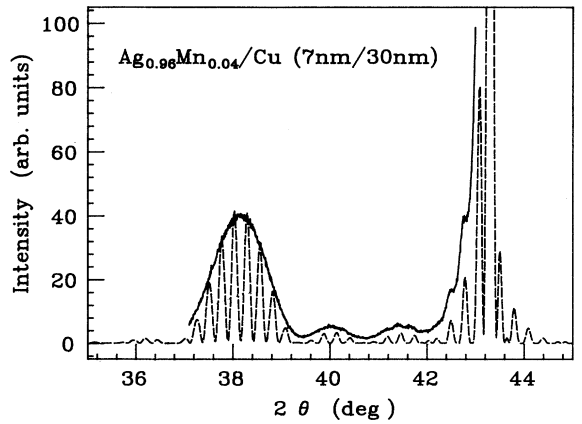

FIG. 4. The LAXD pattern for a $Ag_{0.96}Mn_{0.04}/Cu$ (7-nm/30-nm) MS compared with the calculated pattern for a rectangular model with (7.1 nm)/(28.6 nm). The short coherence length nearly washed out the $1/d$ oscillations [from Cowen *et al.* (Ref. 19)].

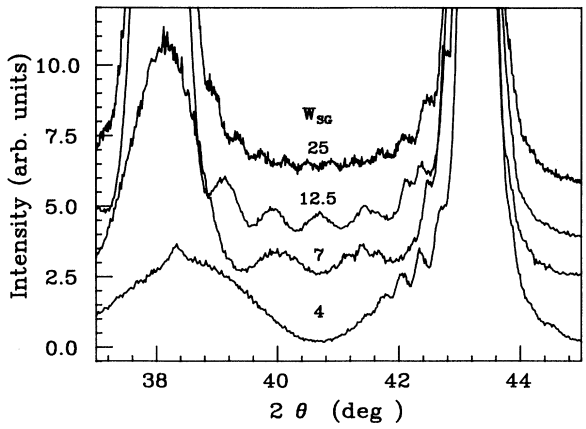

FIG. 5. LAXD patterns for a series of $Ag_{0.96}Mn_{0.04}/Cu$ (W_{SG}/30-nm) MS's, showing how the "diffraction" pattern varies as W_{SG} increases. The separation between the diffraction peaks determines W_{SG}^{M}.

cillations are nearly washed out, so that the region between the large Ag-Mn and Cu peaks is dominated by the two broad "diffraction" maxima due to W_{SG}. Figure 5 shows how the separation between these maxima grows as W_{SG} decreases.

III. EXPERIMENTAL DATA AND ANALYSIS

A. $\chi(T)$

Measurements of χ vs T were made on a Quantum Design MPMS superconducting quantum interference device (SQUID) magnetometer. This apparatus is capable of measuring sample magnetic moments over a wide range of temperatures and magnetic fields with a resolution of $\approx 1\times10^{-8}$ emu.

To measure χ for our layered samples, the sample plus substrate was cut into 0.5-cm×1-cm strips to fit into the measuring coils. The magnetic field was set to zero and the sample was cooled from well above the expected T_f down to 5 K. The magnetic field was then raised to the measuring value of $H=100$ G, and $\chi=M/H$ measurements were taken at a series of increasing temperatures, with measuring time $\sim$5 minutes per data point. The resulting data are called the zero-field-cooled (ZFC) data. With the field held at 100 G, measurements were then taken either at a series of decreasing temperatures back down to 5 K, or the sample was again cooled to 5 K and then warmed again. Such data are called field-cooled (FC) data; little or no differences were found between data taken with the two different FC procedures. Occasional checks showed that T_f was independent of H for $H \leq 100$ G.

Figure 6 shows ZFC data for a series of $Ag_{0.96}Mn_{0.04}/Ag$ MS's along with one example of FC data. These curves are representative of the susceptibility data of all of the Ag-Mn/Cu or Ag-Mn/Ag MS's, particularly in showing that the characteristic features of spin-

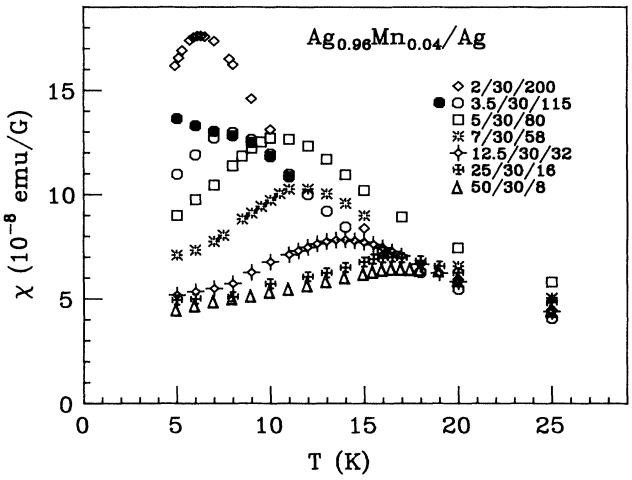

FIG. 6. ZFC χ_{dc} versus T for a series of $Ag_{0.96}Mn_{0.04}/Ag$ (W_{SG}/30-nm) MS's, showing how the data continue to display the characteristic form of a SG down to the thinnest values of W_{SG} studied, and that T_f (the location of the maximum in each curve) decreases monotonically with decreasing W_{SG}. The filled circles show the FC curve for the 3.5-nm/30-nm sample. The numbers at the right of the graph represent W_{SG} (in nm), $W_{il}=30$ nm, and the total number of layers in the MS.

glasses persist right down to the thinnest layers we have studied.

Starting from $T\approx 5$ K, the ZFC susceptibility increases with increasing temperature up to a maximum, the temperature of which is designated as T_f. Above T_f, the ZFC χ exhibits Curie-like behavior.

The FC χ is also Curie-like above T_f, but typically slightly larger than the ZFC χ at the same temperature. In bulk spin-glass materials, the FC χ typically first decreases slightly as T is reduced below T_f, and thereafter remains nearly constant.[17] In our Ag-Mn–based MS's, and FC χ also typically decreases slightly as T is reduced below T_f, but then increases as $T\rightarrow 0$ K.[4] Similar behavior was previously seen in Cu-Mn/Cu MS's.[4]

For the Ag-Mn/Ag MS's, the susceptibilities for $T>T_f$ all appear to follow generally similar Curie-like behavior, with magnitudes corresponding to approximately the same number of paramagnetic moments. This is what we would expect, since we have attempted to keep the total amount of SG material about the same in all of the samples. Part of the residual differences in χ can be attributed to differences in the (nearly temperature independent) susceptibilities of the diamagnetic Si substrates backing the samples, for which no correction has been made. But it is not clear that this is the complete explanation, since remeasurements of Cu-Mn—based MS's[23] after several months have shown that, while T_f for a given sample remains constant, the magnitudes of both the ZFC and FC χ's, as well as the separations between them, can change.

From Fig. 6, we see that T_f decreases systematically with decreasing W_{SG}. By fitting a smooth curve to the data in the vicinity of each peak, the uncertainty in T_f could be reduced to ± 0.5 K.

B. Magnetic decoupling of SG layers

To determine what interlayer thicknesses W_{il} of Cu or Ag were large enough to magnetically decouple the SG layers from each other, Cu-Mn– and Ag-Mn–based MS's with fixed $W_{SG}=4$ nm were prepared with W_{il} up to 120 or 60 nm, respectively. For both types of MS, T_f was found to become independent of W_{il}—to within experimental uncertainty—for $W_{il}\geq 30$ nm.[4,18,19] Figure 7 illustrates this behavior for the $Ag_{0.91}Mn_{0.09}/Cu$ MS.

TABLE IV. Values of T_f for the $Ag_{0.96}Mn_{0.04}/Ag$, $Ag_{0.96}Mn_{0.04}/Cu$, and $Ag_{0.91}Mn_{0.09}/Cu$ MS's with $500\geq W_{SG}\geq 1$ nm, along with the values obtained for target shavings. The uncertainty in the determination of T_f for a given sample or for the shavings is ± 0.5 K. The values listed for $W_{SG}=500$ nm are averages over samples made on different runs, and their uncertainties indicate the variations observed.

	$Ag_{0.96}Mn_{0.04}/Cu$		$Ag_{0.96}Mn_{0.04}/Ag$		$Ag_{0.91}Mn_{0.09}/Cu$	
W_{SG}	(a)	(b)	(a)	(b)	(a)	(b)
Shavings			27.5			45.0
400–1000 films			16.5±1			26.0±1
500					22.7	
200					24.1	
100	17.3	17.7	19.3	18.5	25.7	
50	17.5	16.9	16.3	17.2	22.8	
25	15.9	16.7	16.7	16.6	22.8	
12.5	14.2	14.5	13.5	13.9	17.2	19.0
7	12.2	12.1	11.5	11.8	15.5	17.1
5	10.0	11.1	10.6	10.5	12.6	14.4
4						13.1
3.5	8.35	8.1	7.8	7.9	10.7	12.3
2	5.35	5.5	6.0	6.3	6.8	7.8
1					4.5	5.0

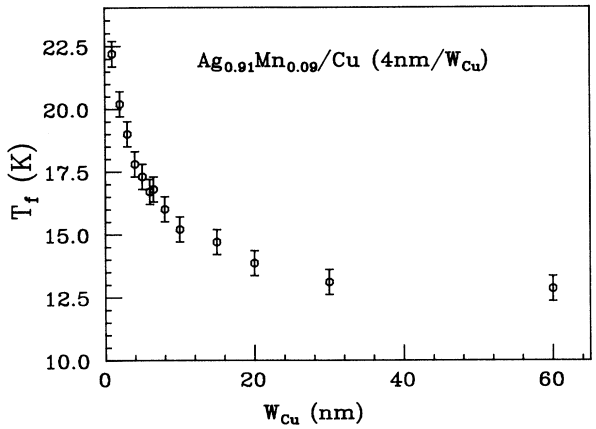

FIG. 7. T_f versus W_{il} for a series of $Ag_{0.91}Mn_{0.09}$/Cu (4-nm/W_{il}) MS's, showing that T_f becomes independent of W_{il} beyond $W_{il} \approx 30$ nm. The error bars represent uncertainties of ± 0.5 K.

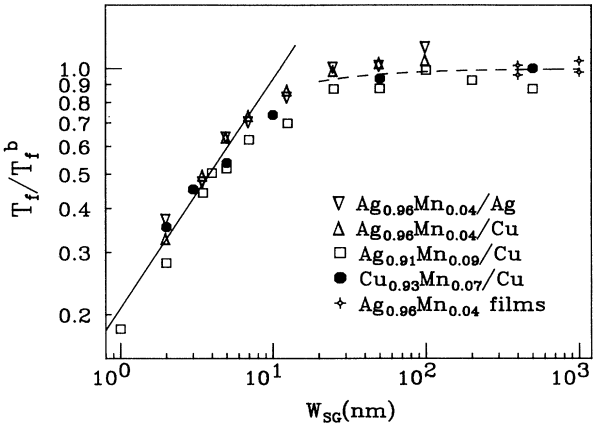

FIG. 8. $\log T_f/T_f^b$ versus $\log W_{SG}$ for a variety of W_{SG}/30-nm MS's and a few thick $Ag_{0.96}Mn_{0.04}$ films, showing that the data for the Ag-Mn–based MS's fall closely around those for the Cu-Mn–based MS's. The plotted values of T_f for the Ag-Mn MS's are averages of those listed in Table IV. The dashed line indicates the behavior predicted by Eq. (1) with $\nu = 1.2$. The solid line indicates behavior compatible with Eq. (4) for $a = 0.65$.

C. T_f and T_f/T_f^b for magnetically isolated SG layers

Table IV contains the values of T_f for all of our Ag-Mn MS's, along with values measured from shavings from each of the two targets. As noted above, the values of T_f for 400–1000-nm-thick films are chosen as T_f^b.

For simplicity, we plot only the averaged values of T_f for MS's prepared together. Figure 8 shows these averaged values in the form $\log T_f/T_f^b$ vs $\log W_{Cu\text{-}Mn}$ for the $Ag_{0.96}Mn_{0.04}$/Ag (inverted triangles), $Ag_{0.96}Mn_{0.04}$/Cu (erect triangles), and $Ag_{0.91}Mn_{0.09}$ (squares) MS's, along with a few values for $Ag_{0.96}Mn_{0.04}$ single films (open crosses) and data for a $Cu_{0.93}Mn_{0.07}$/Cu MS's (filled circles) from Ref. 4. the logarithmic scale for $W_{Cu\text{-}Mn}$ permits display on a single graph of data for $W_{Cu\text{-}Mn}$ ranging from 1000-nm down to 1 nm. The logarithmic scale for T_f/T_f^b permits direct visual determination of whether the data for thin samples are compatible with Eq. (4). The data for all four sample sets are the same to within experimental uncertainties, which are usually dominated by the uncertainties in T_f^b.

The dashed curve in Fig. 8 corresponds to the fit to Eq. (1) previously obtained with Cu-Mn–based MS's.[4] The substantial uncertainties in T_f^b for the present samples preclude an independent fit to this equation, but we see that the Ag-Mn–based data cluster around the previous fit. The solid line in Fig. 8 corresponds to Eq. (4). The slope of this line, $a = 0.65 \pm 0.1$, is slightly larger than the value $a = 0.5 \pm 0.1$ previously reported for Cu-Mn/Cu MS's[4] but still compatible with the rough estimates of a given in Sec. I. We noted in Sec. I that the Cu-Mn/Cu MS data extended down to only $T_f/T_f^b \approx 0.3$, and thus that only the thinnest SG layers were beginning to satisfy the validity condition of Eq. (4): $T_f/T_f^b \ll 1$. The Ag-Mn data of Fig. 8 extend down to $T_f/T_f^b \approx 0.2$, further into the expected region of validity of Eq. (4), and this extension accounts for their larger value of a.

IV. SUMMARY AND CONCLUSIONS

(1) From comparison of values of T_f for 400–1000-nm-thick sputtered film's with those for shavings from the Ag-Mn targets, we infer that the Mn concentration in the Ag-Mn–based MS's is only about 60% of that in target. We attribute this smaller Mn concentration in the MS's primarily to greater scattering of the lighter Mn atoms by the sputtering gas. The reproducibility of our data for very different samples indicates that this Mn concentration must be nearly the same for all of our MS.

(2) Typical SG characteristics (i.e., a peak in ZFC χ and irreversability below T_f) persist to SG layer thicknesses down to at least $W_{SG} = 1$ nm.

(3) To within experimental uncertainties, T_f/T_f^b is the same for a given value of W_{SG} for both Ag-Mn/Ag and Ag-Mn/Cu MS's over the range of W_{SG} studied. The SG properties of these MS are thus not significantly affected by the different grain sizes and interface structures arising from the different lattice parameters of Ag and Cu.

(4) In agreement with the behavior previously found for $Cu_{1-x}Mn_x$/Cu MS's, to within experimental uncertainties, T_f/T_f^b is independent of Mn concentration for $Ag_{0.96}Mn_{0.04}$ and $Ag_{0.91}Mn_{0.09}$ MS's.

(5) T_f/T_f^b is also the same to within experimental uncertainties for Cu-Mn and Ag-Mn–based MS's. Finite size effects are thus very much the same in these two similar SG's.

(6) The data for both thick and thin SG layers are compatible with the Fisher-Huse model, with the thin sample data yielding an exponent in Eq. (4) of $a = 0.65 \pm 0.1$. This value is at the upper end of the range derived from independent estimates of the coefficients in Eq. (3), but well below the rigorous upper bound of 2. However, not

all of the data used to determine this value lie within the range of expected validity of Eq. (4).

(7) We show that, under certain circumstances, LAXD measurements on MS can directly yield the thickness of the thinner layer in an MS.

We conclude that our data for magnetically decoupled Ag-Mn–based MS's behave very similarly to those previously reported for Cu-Mn–based MS's.

ACKNOWLEDGMENTS

This research was supported in part by the U.S. NSF under Grant No. DMR-88-19429, by the MSU Center for Fundamental Materials Research, and by the Swiss National Science Foundation through partial support for one of us (R.S.). The authors thank J. Mattsson for helpful discussions.

*Present address: Department of Physics, University of Lausanne, CH-1015 Lausanne, Switzerland.

[1]A. Fert (unpublished)

[2]G. G. Kenning, J. M. Slaughter, and J. A. Cowen, Phys. Rev. Lett. **59**, 2596 (1987).

[3]J. A. Cowen, G. G. Kenning, and J. Bass, J. Appl. Phys. **64**, 5781 (1988).

[4]G. G. Kenning, J. Bass, W. P. Pratt, Jr., D. Leslie-Pelecky, L. Hoines, W. Leach, M. L. Wilson, R. Stubi, and J. A. Cowen, Phys. Rev. B **42**, 2393 (1990).

[5]A. Gavrin, J. R. Childress, C. L. Chien, B. Martinez, and M. B. Salamon, Phys. Rev. Lett. **64**, 2438 (1990).

[6]J. A. Cowen, G. G. Kenning, and J. M. Slaughter, J. Appl. Phys. **61**, 4080 (1987).

[7]M. N. Barber, in *Phase Transitions and Critical Phenomena,* edited by C. Domb and J. L. Lebowitz (Academic, New York, 1983), Vol. 8.

[8]L. P. Lévy and A. T. Ogielski, Phys. Rev. Lett. **57**, 3288 (1986).

[9]R. Stubi, J. A. Cowen, D. Leslie-Pelecky, and J. Bass, Physica B **165&166**, 459 (1990).

[10]J. Vranken, C. Van Haesendonck, H. Vloeberghs, and Y. Bruynseraede, Phys. Scr. **T25**, 348 (1989).

[11]H. Vloeberghs, J. Vranken, C. Van Haesendonck, and Y. Bruynseraede, Europhys. Lett. **12**, 557 (1990).

[12]D. S. Fisher and D. A. Huse, Phys. Rev. B **36**, 8937 (1987).

[13]A. J. Bray and M. A. Moore, J. Phys. C **17**, L463 (1984); W. L. McMillan, Phys. Rev. B **30**, 476 (1984); W. Kinzel and K. Binder, Phys. Rev. B **29**, 1300 (1984); A. P. Young, Phys. Rev. Lett. **50**, 917 (1983); C. Dekker, A. F. M. Arts, H. W. de Wijn, A. J. van Duyneveldt, and J. A. Mydosh, *ibid.* **61**, 1780 (1988); J. Mattson, P. Granberg, P. Nordblad, and L. Lundgren (unpublished).

[14]L. Sandlund, P. Granberg, L. Lundgren, P. Nordblad, P. Svedlindh, J. A. Cowen, and G. G. Kenning, Phys. Rev. B **40**, 869 (1989). P. Granberg, P. Nordblad, P. Svedlinch, L. Lundgren, R. Stubi, G. G. Kenning, D. L. Leslie-Pelecky, J. Bass, and J. A. Cowen, J. Appl. Phys. **67**, 5252 (1990).

[15]J. Mattsson, P. Granberg, P. Nordblad, L. Lundgren, R. Stubi, D. Leslie-Pelecky, J. Bass, and J. Cowen, Physica B **165&166**, 461 (1990).

[16]K. H. Fischer, *Landolt-Börnstein Tables,* New Series, Gruppe III, Vol. 15a, edited by K. H. Hellwege (Springer-Verlag, Berlin, 1982), p. 289.

[17]K. Binder and A. P. Young, Rev. Mod. Phys. **58**, 801 (1986).

[18]L. Hoines, R. Stubi, R. Loloee, J. A. Cowen, and J. Bass, Phys. Rev. Lett. **66**, 1224 (1991).

[19]R. Stubi, D. L. Leslie-Pelecky, and J. A. Cowen, J. Appl. Phys. **67**, 5970 (1990); R. Stubi, J. Bass, and J. A. Cowen, J. Appl. Phys. **69**, 5054 (1991); J. A. Cowen, J. Bass, P. Granberg, L. Lundgren, and R. Stubi, Physica B **69**, 299 (1991)

[20]S. Werner, Commun. Solid State Phys. **15**, 55 (1990).

[21]C. Fierz, R. Stubi, and W. P. Pratt, Jr. (unpublished).

[22]W. B. Pearson, *A Handbook of Lattice Spacings and Structures of Metals and Alloys* (Pergamon, New York, 1958).

[23]D. Leslie-Pelecky (unpublished).